



CrossMark  
click for updates

Cite this: *RSC Adv.*, 2016, 6, 94

## Effective removal of Cr(vi) using $\beta$ -cyclodextrin–chitosan modified biochars with adsorption/reduction bifunctional roles

Xixian Huang,<sup>ab</sup> Yunguo Liu,<sup>\*ab</sup> Shaobo Liu,<sup>\*cd</sup> Xiaofei Tan,<sup>ab</sup> Yang Ding,<sup>ab</sup> Guangming Zeng,<sup>ab</sup> Yaoyu Zhou,<sup>ab</sup> Mingming Zhang,<sup>ab</sup> Shufan Wang<sup>ab</sup> and Bohong Zheng<sup>d</sup>

In this work, beta-cyclodextrin–chitosan modified walnut shell biochars ( $\beta$ -CCWB) were synthesized as a low-cost adsorbent for the removal of heavy metal Cr(vi) from aqueous solutions. Batch sorption experiments were carried out to investigate the adsorption characteristic of  $\beta$ -CCWB. The experimental data fitted a pseudo-second order equation and Freundlich isotherm model, and the optimum adsorption of the modified biochar was observed at pH 2.0 with an adsorption capacity of 206 mg g<sup>-1</sup>. Thermodynamic analysis showed that the adsorption process was spontaneous and endothermic. The removal efficiency of Cr(vi) by  $\beta$ -CCWB (about 93%) was higher than that by the pristine biochar (about 27%). Characteristic analysis indicated that amino and carboxyl groups were the major functional groups for Cr(vi) sorption, and implied that the electrostatic attraction of Cr(vi) to the positively charged biochar surface, reduction of Cr(vi) to Cr(III) ions and the complexation between Cr(III) ions and  $\beta$ -CCWB functional groups were responsible for Cr(vi) removal mechanism in this research. Furthermore, the environmentally friendly and low-cost  $\beta$ -CCWB could be applied as a potential effective adsorbent to remediate Cr(vi) contamination from aqueous solution.

Received 31st October 2015  
Accepted 11th December 2015

DOI: 10.1039/c5ra22886g

[www.rsc.org/advances](http://www.rsc.org/advances)

### 1. Introduction

Due to the development of industry and economy, chromium (Cr) has been commonly used as well as released to the environment in a variety of industrial activities including electroplating, chromate manufacturing, leather tanning,<sup>1,2</sup> electroplating, metal polishing *etc.*<sup>3,4</sup> In contrast to organic contaminants, Cr is non-biodegradable and persistent in ecosystems.<sup>5</sup> Cr exists mainly as Cr(vi) and Cr(III), while the former is much more soluble and mobile in aqueous solutions than the latter, which has caused extensive attention due to its carcinogenic, mutagenic and teratogenic effects on biological systems.<sup>2</sup> Therefore, it is imperative to remove Cr(vi) from wastewater prior to the discharge into water bodies.

All kinds of techniques have been applied to remove Cr(vi) from the aqueous solution, such as cyanide treatment, electro-

chemical precipitation, reverse osmosis,<sup>6</sup> adsorption,<sup>7</sup> solvent extraction and ion exchange.<sup>1,8</sup> Among these methods, adsorption is the most widely used because of its high efficiency and recovery of toxic and valuable metals from wastewater.<sup>9–11</sup> Some adsorbents like activated carbon,<sup>12</sup> zeolite,<sup>13</sup> iron oxide, fullerene,<sup>14</sup> graphene<sup>15</sup> have been used for Cr(vi) removal. However, these materials mentioned above have the defects of limited adsorption ability, aggregation or high cost.

Biochar is the porous carbonaceous by-product generated from biomass through pyrolysis/carbonization under anoxic and anaerobic conditions.<sup>16</sup> When applied to soils, biochar can not only increase soil fertility, raise agriculture productivity and enhance soil water holding capacity,<sup>17,18</sup> but also serve as carbon storage to reduce CO<sub>2</sub> emissions and mitigate climate change.<sup>19</sup> Apart from soil application, recent studies have focused on biochar's potential ability on removing various contaminants (heavy metal, organic pollutants and microbial contaminants) from wastewater system, due to its accessible and abundant in feedstock materials.<sup>20,21</sup> However, the biochar derived directly from biomass feedstock without any modification and activation usually has relatively low adsorption capacity, which is influenced by the feedstock type, production methods and processing conditions.<sup>22,23</sup> Thus, recent researches have paid attention to modify the biochar production process or impregnate the materials with chemical agents so as to improve biochar sorption ability.<sup>24</sup>

<sup>a</sup>College of Environmental Science and Engineering, Hunan University, Changsha 410082, P. R. China. E-mail: [hnluyunguo@163.com](mailto:hnluyunguo@163.com); Fax: +86 731 88822829; Tel: +86 731 88649208

<sup>b</sup>Key Laboratory of Environmental Biology and Pollution Control, Hunan University, Ministry of Education, Changsha 410082, P. R. China

<sup>c</sup>School of Metallurgy and Environment Central South University, Central South University, Changsha 410082, P. R. China. E-mail: [liushaobo23@aliyun.com](mailto:liushaobo23@aliyun.com); Fax: +86 731 88871071; Tel: +86 731 88830923

<sup>d</sup>School of Architecture and Art Central South University, Central South University, Changsha 410082, P. R. China

Chitosan (beta 1,4-polyglucosamine), a renewable transformed polysaccharide and generally prepared commercially by deacetylation of chitin from crustacean shells with alkaline solution, which is one of the most abundant amino-polysaccharide exist in the environment. Chitosan and its derivatives which obtained through chemical and physical modifications of raw chitosan, including cross-linking, grafting and impregnation of the chitosan backbone<sup>25,26</sup> have been used in treating contaminants due to its surface functionalities, biodegradability, nontoxicity and its useful tendency to dissolve in acid solution.<sup>11</sup> Additional, this natural biopolymer and derivatives have received great attention in their application for metal ions adsorption due to the high ratio of amine groups ( $-\text{NH}_2$ ) and hydroxyl groups ( $-\text{OH}$ ) and the insertion of active agents with functional groups into chitosan may make its adsorption capacity to a higher degree.<sup>27</sup> Beta-cyclodextrin ( $\beta$ -CD) has a cylindrical structure, which ends with a hydrophilic exterior and a hydrophobic cavity, which can form inclusion complexes with a wide range of organic molecules possessing suitable shape and size in water spontaneously.<sup>28,29</sup> Thus, the combination of chitosan,  $\beta$ -CD and biochar would be an innovative and effective adsorbent in the treatment of industrial wastewater and nature water.

In this study,  $\beta$ -cyclodextrin–chitosan ( $\beta$ -CC) was synthesized firstly, and then combined with walnut shell biochar produced through slow pyrolysis at different temperatures of 300, 450 and 600 °C, and this new-type materials was used to enhance the adsorption capacity for  $\text{Cr}(\text{vi})$  removal in wastewater. The overarching targets of this study are to: (a) prepare  $\beta$ -cyclodextrin–chitosan walnut shell biochar materials and characterize them; (b) compare the adsorption capacity of modified biochar under different pyrolysis temperature; (c) examine the influence of pH, initial concentration, contact time and ionic strength conditions on the sorption of  $\text{Cr}(\text{vi})$  on this materials; (d) establish and elucidate the underlying interaction mechanisms through a series of laboratory experiments and mathematical model.

## 2. Materials and methods

### 2.1 Materials

Walnut shell biomass was obtained from Changsha, Hunan Province of China. The biomass feedstock were dried and milled to fraction.  $\beta$ -CD with purity above 98% and chitosan with purity above 99% without any further purification were purchased from Beijing Solarbio Science & Technology Co. Ltd. All other chemicals employed in this experiments including HCl, NaOH, NaCl,  $\text{K}_2\text{Cr}_2\text{O}_7$ ,  $\text{H}_2\text{SO}_4$ ,  $\text{H}_3\text{PO}_4$ , acetone, glutaraldehyde, 1-ethyl-3-(3-dimethyl)aminopropyl carbodiimide (EDC), *N*-hydroxyl succinimide (NHS) were of analytical reagent grade.

### 2.2 Preparation of adsorbent

Walnut shell biomass was rinsed with ultrapure water and oven-dried at 60 °C. Then, the dried biomass were pyrolyzed in a lab-scale tubular reactor (SK-G08123K, China) at 300 °C, 450 °C, 600 °C, respectively, in  $\text{N}_2$  environment for 2 h before cooling. The biochar samples produced from different pyrolysis temperature

were referred to as WB300, WB450, WB600, respectively. The samples were then washed, dried (80 °C), and sieved through 150 mesh screen.  $\beta$ -CC was prepared according to the method of Fan *et al.*<sup>30,31</sup> And the  $\beta$ -CC was held by hydrogen binding, with very large surface area and showed great improvement in the uptake properties of contaminants compared to the unmodified chitosan due to its high concentration of active sites. Firstly, WB300, WB450, WB600 biochar dispersion was prepared by sonicating 2 g biochar sample for 2 h in ultrapure water, respectively. Subsequently, the mixed solution (50 mL 0.1 mol  $\text{L}^{-1}$  EDC and 0.1 mol  $\text{L}^{-1}$  NHS) was added into the biochar dispersion with continuous stirring for 2.5 h in order to activate the functional groups of walnut shell biochar. The pH of the resulting solution was adjusted at 7.0 using dilute sodium hydroxide. After that,  $\beta$ -CC (4 g), the activated biochar solution and 10 mL glutaraldehyde were added into a flask and dispersed in ultrapure water by ultrasonic dispersion for 10 min. After ultrasonic dispersion, the mixed solutions were stirred at 60 °C for 2 h. The precipitate was washed with 2% (w/v) NaOH and ultrapure water in turn until pH was about 7.0. Then products were collected through filtration, oven-dried under vacuum overnight at 50 °C and sealed in a desiccator for further experiment tests. The obtained novel composites are referred to as  $\beta$ -CCWB300,  $\beta$ -CCWB450 and  $\beta$ -CCWB600.

### 2.3 Characterization of biochar

The BET and pore volume analysis was carried out with the Brunauer, Emmett, and Teller (BET) (Instruments Quadrasorb SI, USA). Scanning electron microscope (SEM) images were obtained on a field emission scanning electron microscopy (JSM-7001F, Japan). Fourier transform infrared (FTIR) spectrum was measured on a spectrophotometer (Nicolet Magna-IR 750 spectrometer, USA) using the KBr pellet technique. The X-ray photoelectron spectroscopy (XPS) measurements were performed using an ESCALAB 250Xi X-ray photoelectron spectrometer (Thermo Fisher, USA).

### 2.4 Batch adsorption of $\text{Cr}(\text{vi})$

The adsorption of  $\text{Cr}(\text{vi})$  was studied as a function of pH, initial concentration, contact time, adsorption temperature, and ionic strength. Potassium dichromate ( $\text{K}_2\text{Cr}_2\text{O}_7$ ) was used for preparing the stock solutions of heavy metals. The concentrations of residual  $\text{Cr}(\text{vi})$  were analyzed by measuring the absorbance of the purple complex of  $\text{Cr}(\text{vi})$  with 1,5-diphenylcarbohydrazide method with a UV-vis spectrophotometer (Pgeneral T6, Beijing, China) at the wavelength of 540 nm.

In order to investigate the effect of initial solution pH in this adsorption, the initial pH values of 50 mL  $\text{Cr}(\text{vi})$  solution (100 mg  $\text{L}^{-1}$ ) were adjusted from 2.0 to 10.0 using dilute NaOH or HCl solutions. Kinetic tests were carried out by contacting 0.1 g adsorbent with 50 mL  $\text{Cr}(\text{vi})$  solution (100 mg  $\text{L}^{-1}$ ) at 25 °C and optimum pH value of 2.0 in thermostatic water bath oscillators. The residual  $\text{Cr}(\text{vi})$  concentration was measured after designated time period (5, 10, 30, 60, 120, 240, 360, 480, 720, 960, 1200, 1440, 1800, 2280 and 2800 min). For the adsorption isotherm study, 0.1 g of adsorbent was contacted with 50 mL of

Cr(vi) solution at concentrations of 20, 50, 100, 200, 300, 400, 500, 600 and 800 mg L<sup>-1</sup> at 25 °C with continuous shaking. For the effect of background ionic strength, the experiments were studied at pH 2.0, 25 °C and initial Cr(vi) solution (100 mg L<sup>-1</sup>) was adjusted by different concentrations of NaCl (0, 0.001, 0.005, 0.01, 0.05, 0.1, 0.5, 1.0 mol L<sup>-1</sup>). The removal percentage (*p*, %) and the equilibrium adsorption capacity (*q<sub>e</sub>*, mg g<sup>-1</sup>) of β-CCWB450 was calculated by using the following equations:

$$p = \frac{C_0 - C_e}{C_0} \times 100\% \quad (1)$$

$$q_e = \frac{V(C_0 - C_e)}{m} \quad (2)$$

where *C<sub>0</sub>* (mg L<sup>-1</sup>) and *C<sub>e</sub>* (mg L<sup>-1</sup>) are the initial and equilibrium concentrations of Cr(vi) ions, *m* (g) is the mass of the adsorbent β-CCWB450 and *V* (L) is the volume of metal solution.

All the experimental treatments were performed in duplicate and the average values were reported. The relative errors of the data were generally within 5%.

### 3. Results and discussion

#### 3.1 Characteristic of β-CCWB

**3.1.1 BET and pore volume.** The surface area, pore volume and pore size of WB450 and β-CCWB450 were presented in Table 1. The BET surface area of β-CCWB450 (82.09 m<sup>2</sup> g<sup>-1</sup>) was larger than that of pristine biochar (11.76 m<sup>2</sup> g<sup>-1</sup>), and the β-CCWB450 was possessed of larger pore volume and smaller pore size than that of WB450. This phenomenon may be due to the process of introducing β-CC.

**3.1.2 SEM.** The surface morphological characteristics of the materials before and after heavy metal adsorption were compared by the scanning electron microscopy graphs. The SEM images of the carbon materials are presented in Fig. 1. As seen in Fig. 1a, a lot of carbon particles were observed from the surface of the pristine biochar (WB450), which indicated that the walnut shell were pyrolyzed and carbonized. As shown in Fig. 1b, the β-CC spheres were decorated and anchored on the surface of WB450, which provided effective adsorption sites and generated higher BET surface areas and larger pore volume. Fig. 1c showed that the pore amount decreased and some splendid crystals appeared on the surface of β-CCWB450 after the adsorption of Cr(vi). This may be that chromium ions were adsorbed on it and blocked the pore channel.

**3.1.3 FTIR.** The FTIR of WB450 and β-CCWB450 (before and after adsorption) were shown in Fig. 2. Obviously, the characteristic peak around 3423 cm<sup>-1</sup> was ascribed to the

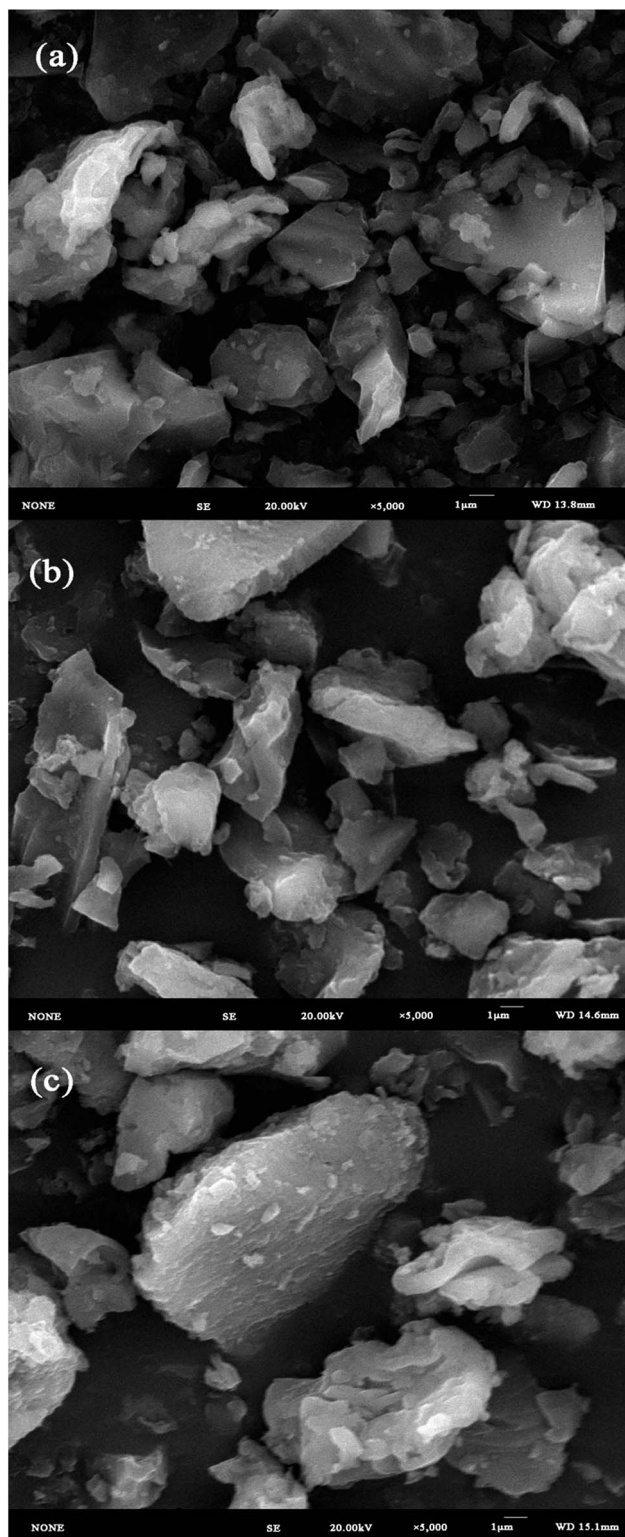


Fig. 1 SEM images of (a) pristine biochar, (b) modified biochar before adsorption and (c) after adsorption.

Table 1 BET characteristics of β-CCWB450 and WB450

|           | Specific surface area (m <sup>2</sup> g <sup>-1</sup> ) | Pore volume (m <sup>3</sup> g <sup>-1</sup> ) | Average pore (nm) |
|-----------|---|---|-------------------|
| WB450     | 11.76   | 0.02589                                       | 8.805             |
| β-CCWB450 | 82.09   | 0.08271                                       | 4.030             |

bound water and nitrogen hydrogen band in the samples,<sup>32</sup> illustrating that some amino groups and hydroxyl groups were formed on the surface of the pristine materials. The broad adsorption peak at 2937 cm<sup>-1</sup> was mainly attributed to



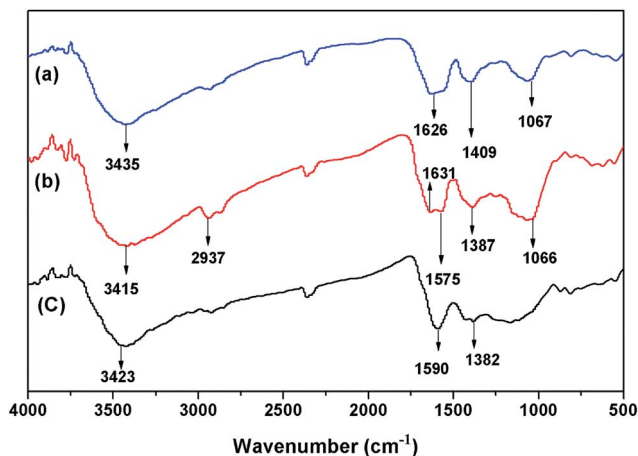


Fig. 2 FTIR spectra of (a) WB450 and (b)  $\beta$ -CCWB450 before adsorption and (c) after adsorption.

the CH- and CH<sub>2</sub>- stretching vibrations.<sup>8</sup> The broad band of 1590 cm<sup>-1</sup> and 1575 cm<sup>-1</sup> was mainly assigned to the stretching vibration of O-H and C=O stretching vibrations of ester in pristine biochar.<sup>9</sup> The new broad band detected on modified biochar (Fig. 2b and c) at 1625–1635 cm<sup>-1</sup> represent the stretching vibrations of O-H and C=O stretching vibrations of ester in chitosan. The absorbance band near 1387 cm<sup>-1</sup> was related to -CH symmetric bending vibrations in -CHOH-. The peak at 1066 cm<sup>-1</sup> was the C-O bending vibration in -COH.<sup>30</sup>

In a word, the groups of -NH<sub>2</sub>, -OH, COO<sup>-</sup>, C-O and H-O-H changed after modification, which was attributed to the introduction of  $\beta$ -CC. The bending vibration of -NH<sub>2</sub> and COO<sup>-</sup> shifted to the lower frequencies after Cr(vi) adsorption. These changes indicated that the amino and carboxyl groups could be the main functional groups for Cr(vi) adsorption. The results were markedly compatible with the previous investigation.<sup>4,33</sup>

**3.1.4 XPS.** The XPS was performed on  $\beta$ -CCWB450 and  $\beta$ -CCWB450 loaded with Cr to study the surface chemical compositions and investigate the species of the Cr bound on the  $\beta$ -CCWB450 to gain further information on its removal mechanism.

The principal elements on the surface of the  $\beta$ -CCWB450 before adsorption were C 1s (77.06%), O 1s (20.69%), N 1s (2.24%), chrome (not been detected because of the extremely low content) and the modified biochar after adsorption were C 1s (66.32%), O 1s (28.46%), N 1s (1.68%) and Cr<sub>2p</sub> (3.53%) (see Fig. 3a). The N/C ratio was estimated to be 0.29 and 0.25 for  $\beta$ -CCWB450 before and after adsorption, respectively. The obvious increase in chrome content and the decrease in N/C ratio indicated that  $\beta$ -CC was introduced into biochar and amino groups may participate in removing chromium ions.

Detailed XPS survey of the regions for trivalent chromium and hexavalent chromium was shown in Fig. 3b. The area of Cr(III) peak at the binding energy of 577.5 eV is distinctly greater than the area of Cr(vi) peak at the binding energy of 579.3 eV. This data demonstrated that part of adsorbed Cr(vi) anions was reduced to Cr(III) after exposure to  $\beta$ -CCWB450.

As shown in Fig. 3c, the C 1s XPS spectrum of  $\beta$ -CCWB450 can be curve-fitted into three peak components at approximately 284.8 eV (C-C), 286.9 eV (C-O) and 288.1 eV (C=O).<sup>34,35</sup> As seen from Fig. 3d, the C 1s XPS spectrum of  $\beta$ -CCWB450 loaded with Cr clearly indicates that five components corresponding to C-C (284.8 eV), C-O (286.2 eV), C-Cr (287.1 eV), C=O[Cr(CO)<sub>6</sub>] (287.9 eV) and COO<sup>-</sup> (288.9 eV).<sup>36,37</sup> On the basis of the XPS results, the main difference between  $\beta$ -CCWB450 and  $\beta$ -CCWB450 loaded with Cr was the new peak of C-Cr and COO<sup>-</sup> bond. That may be attributed to the fact that carboxyl groups were successfully introduced to the modified biochar and this functional groups can enhance the ability of modified materials to remove chromium ions by chelation reaction.

The peak around 399 eV was attributed to N 1s (Fig. 3e and f). Following the modification of  $\beta$ -CC, the pristine biochar was functionalized with -NH<sub>2</sub> groups, which was in agreement with FTIR results. In addition, the minor shift in bond energy of quinoid amine (C=N), benzoid amine (C-N) and new peak occurred at 401.1 eV in doped imine (C=N<sup>+</sup>) also revealed that amino groups were involved in the fixation of Cr(vi) and chelation of Cr(III) during the adsorption process.

### 3.2 Comparison of removal efficiency by modified biochar and pristine biochar

The comparison of removal efficiency by  $\beta$ -CCWB300,  $\beta$ -CCWB450,  $\beta$ -CCWB600 and WB450 was carried out at the varying Cr(vi) concentrations from 20 to 800 mg L<sup>-1</sup> at initial pH of 2.0 and temperature of 25 °C.

As shown in Fig. 4a, the Cr(vi) adsorption capacity of the modified biochar from three different pristine biochar were almost equal at diverse Cr(vi) concentration solutions at 298.15 K, which indicating that the pyrolysis temperature has no significant effect on adsorption of Cr(vi) by  $\beta$ -CCWB. However, from Fig. 4b, the Cr(vi) adsorption capacity of the  $\beta$ -CCWB450 ranged from 9.9 mg g<sup>-1</sup> to 136.25 mg g<sup>-1</sup> at 298.15 K and the optimum adsorption was 206 mg g<sup>-1</sup> at 318.15 K, which was much higher than of the pristine biochar (WB450).

In a word, the removal efficiency of the modified biochar was 1.1 to 3.1 times higher than that of the pristine biochar and this novel modified materials  $\beta$ -CCWB exhibited much higher adsorption capacity and removal efficiency than pristine biochar.

### 3.3 The effect of zero point charge and optimization of pH

Zero point charge (pH<sub>pzc</sub>), the potential in the sliding plane of colloidal particles, which is related to the surface charge of particles.<sup>38</sup> The zeta potentials of the  $\beta$ -CCWB450 are shown in Fig. 5. It was obvious that pH<sub>pzc</sub> of the  $\beta$ -CCWB450 was found to be at pH 3.6. Under the solution pH < pH<sub>pzc</sub>, the surface of the  $\beta$ -CCWB450 was positively charged, resulted in the main adsorption mechanism of significant electrostatic attraction between the positively charged surface and the Cr(vi) anions. When the solution pH > pH<sub>pzc</sub>,  $\beta$ -CCWB450 surface was negatively charged, which was due to the deprotonation of functional groups of  $\beta$ -CCWB450 that could inhibit the Cr(vi) adsorption due to electrostatic repulsion between the negative

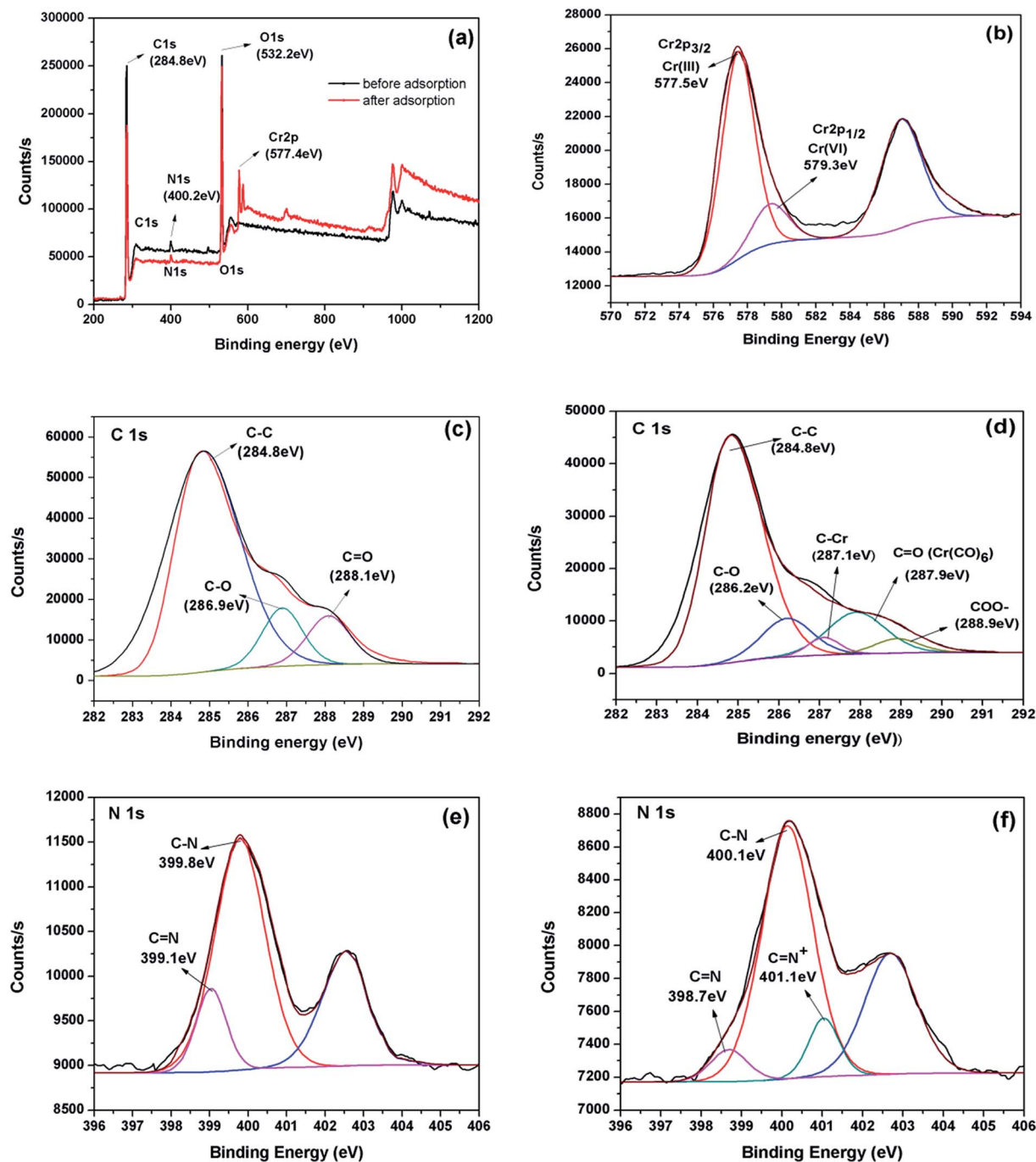


Fig. 3 XPS spectra of (a)  $\beta$ -CCWB450 before and after adsorption, (b) Cr<sub>2p</sub> of  $\beta$ -CCWB450 after adsorption, (c) the C 1s XPS spectra of  $\beta$ -CCWB450 before and (d) after adsorption, (e) the N 1s XPS spectra of  $\beta$ -CCWB450 before and (f) after adsorption.

charge of  $\beta$ -CCWB450 and Cr(vi) anions, suggesting that other sorption mechanism served as the main force to adsorb Cr(vi) such as surface complexation.

pH is one of the most crucial factors significantly affecting the adsorption efficiency. The surface charge and the speciation of chromium depended on the solution pH. Cr(vi) exists primarily as  $\text{HCrO}_4^-$  and  $\text{Cr}_2\text{O}_7^{2-}$  (pH = 1.0–6.8) and stable  $\text{CrO}_4^{2-}$  (pH > 6.8).<sup>39</sup> Cr(III) was predominantly presented as  $\text{Cr}^{3+}$  under acidic condition. During the adsorption, at low pH, more

$\text{HCrO}_4^-$  and  $\text{Cr}_2\text{O}_7^{2-}$  formed and the stronger interaction between the positively charged functional groups of adsorbent and the negatively charged chromate ions caused higher adsorption.<sup>2</sup> Meanwhile, in this process, Cr(vi) was partially reduced to Cr(III) by reductive surface functional groups like amino groups and hydroxyl groups<sup>40</sup> on the  $\beta$ -CCWB. Some Cr(III) released back into the solution in the form of water-soluble Cr(III) species, others precipitated<sup>3</sup> on the surface of the  $\beta$ -CCWB in the form of  $\text{Cr}_2\text{O}_3$ .

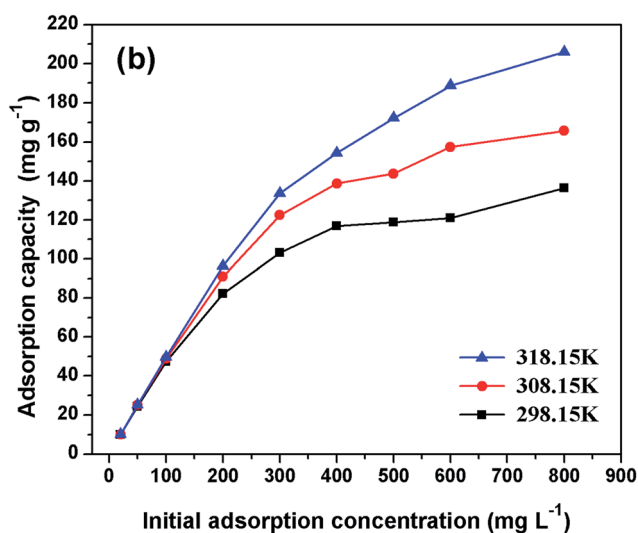
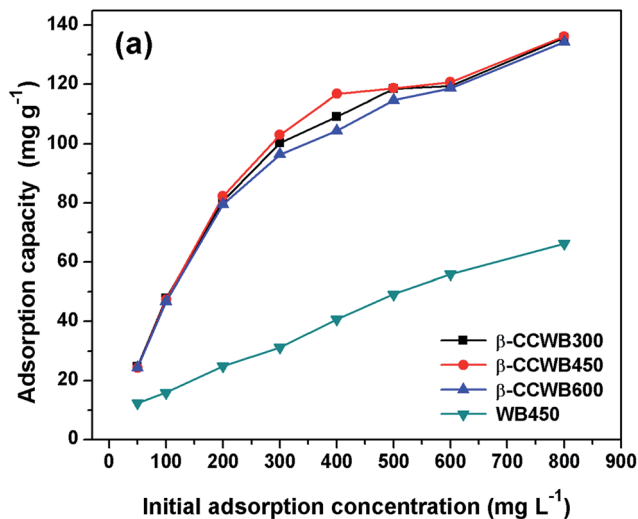


Fig. 4 (a) The comparison of adsorption capacity on  $\beta$ -CCWB and WB450 under 298.15 K, (b) the comparison of adsorption capacity on  $\beta$ -CCWB450 under different adsorption temperatures (Cr(vi) solution volume: 50 mL; adsorbent dose: 0.1 g; contact time: 24 h; pH: 2.0).

From Fig. 5, the decrease in Cr(vi) removal with the increase of pH could be attributed to the competition between higher concentration of  $\text{OH}^-$  with Cr(vi) species for the sorption sites on the  $\beta$ -CCWB. From the above, the optimum solution pH was 2 for Cr(vi) removal.

### 3.4 Adsorption experiments

**3.4.1 Adsorption kinetics.** The kinetics of Cr(vi) removal was carried out to understand the adsorption behavior of  $\beta$ -CCWB450. The Cr(vi) adsorption data onto  $\beta$ -CCWB450 was shown in Fig. 6a and the contact time was varied between 5 min to 2880 min to establish equilibrium. The rate of Cr(vi) adsorption was fast, with 80% of the ultimate adsorption occurred in the first 5 min, and the adsorption capacity continued to raise slightly for the next 12 h, followed by a very slow approach to equilibrium.

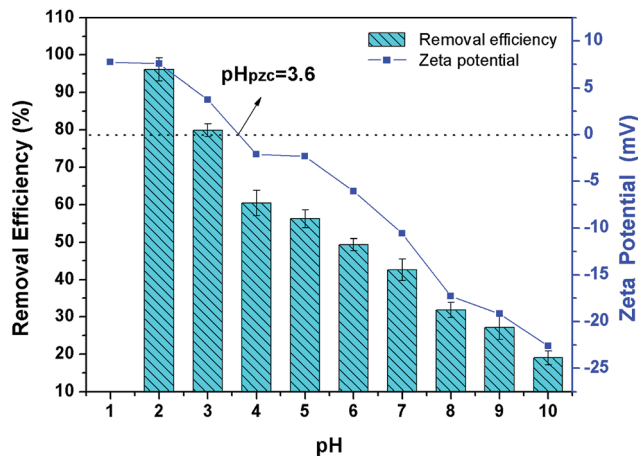


Fig. 5 Effect of initial solution pH values on Cr(vi) removal by  $\beta$ -CCWB450 and zeta potential of  $\beta$ -CCWB450 at different solution pH.

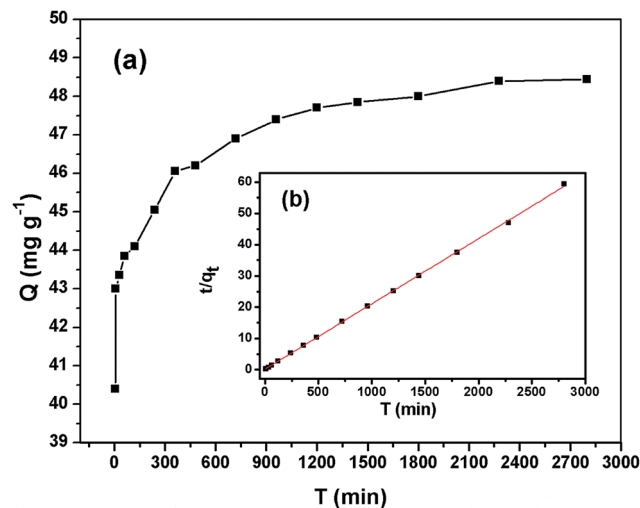


Fig. 6 Kinetics of Cr(vi) adsorption onto the  $\beta$ -CCWB450 at 298.15 K. (a) Cr(vi) sorption kinetics data, (b) pseudo-second-order model for Cr(vi) adsorption (initial Cr(vi) concentration 100  $\text{mg L}^{-1}$ ; pH = 2.0).

To investigate the mechanism of adsorption, three different kinetic models (pseudo-first-order, pseudo-second-order, and Elovich) were applied and illustrated as follows:

The pseudo-first-order model:

$$\log(q_e - q_t) = \log q_e - \frac{k_1}{2.303} t \quad (3)$$

The pseudo-second-order model:

$$\frac{t}{q_t} = \frac{t}{q_e} + \frac{1}{k_2 q_e^2} \quad (4)$$

The Elovich model:

$$q_t = \frac{1}{\beta} \ln(\alpha\beta) + \frac{1}{\beta} \ln(t) \quad (5)$$

Table 2 Pseudo-first-order, pseudo-second-order and Elovich equation model parameters for Cr(vi) adsorption on  $\beta$ -CCWB450

|                     | Parameter 1   | Parameter 2  | $R^2$ |
|---------------------|---|--|-------|
| Pseudo-first-order  | $q_e = 46.60 \text{ mg g}^{-1}$                                   | $k_1 = 0.83 \text{ min}^{-1}$                      | 0.65  |
| Pseudo-second-order | $q_e = 48.50 \text{ mg g}^{-1}$                                   | $k_2 = 0.00015 \text{ g mg}^{-1} \text{ min}^{-1}$ | 0.999 |
| Elovich             | $\alpha = 4.06 \times 10^{15} \text{ mg g}^{-1} \text{ min}^{-1}$ | $\beta = 0.0854 \text{ g mg}^{-1}$                 | 0.959 |

Table 3 Constants and correlation coefficients of Freundlich and Langmuir models for Cr(vi) adsorption onto  $\beta$ -CCWB450

| T (K)  | Langmuir model                   |                                  |       | Freundlich model                 |      |       |
|--------|----------------------------------|----------------------------------|-------|----------------------------------|------|-------|
|        | $q_m \text{ (mg g}^{-1}\text{)}$ | $K_L \text{ (L mg}^{-1}\text{)}$ | $R^2$ | $K_F \text{ (L mg}^{-1}\text{)}$ | $n$  | $R^2$ |
| 298.15 | 124.42                           | 0.091                            | 0.95  | 31.84                            | 4.20 | 0.96  |
| 308.15 | 149.33                           | 0.090                            | 0.95  | 38.83                            | 4.19 | 0.98  |
| 318.15 | 188.56                           | 0.101                            | 0.92  | 52.98                            | 4.29 | 0.99  |

where  $q_e \text{ (mg g}^{-1}\text{)}$  and  $q_t \text{ (mg g}^{-1}\text{)}$  are the amount of metal ion adsorbed per unit mass of the adsorbent at equilibrium and time  $t \text{ (min)}$  respectively.  $k_1 \text{ (min}^{-1}\text{)}$  and  $k_2 \text{ (g mg}^{-1} \text{ min}^{-1}\text{)}$  are the pseudo-first-order and pseudo-second-order rate constant respectively.  $\alpha \text{ (mg g}^{-1} \text{ min}^{-1}\text{)}$  and  $\beta \text{ (g mg}^{-1}\text{)}$  are the Elovich constants.

The results of the above three kinetics were presented in Table 2. The correlation coefficient values were much higher for the pseudo-second-order ( $R^2 = 0.99$ ) (Fig. 6b) than the pseudo-first-order ( $R^2 = 0.65$ ) and Elovich ( $R^2 = 0.96$ ) kinetics model, which suggested that experimental data fitted well with the pseudo-second-order model. So that, the chemisorption of Cr(vi) was the rate-determining step of adsorption process, which involved the chemical interaction between chromium ions and polar functional groups on the adsorbent, such as ion exchange and chelating reaction.

**3.4.2 Adsorption isotherm.** In order to study the adsorption equilibrium of Cr(vi), Langmuir isotherm model and Freundlich isotherm model were applied to simulate the equilibrium characteristics of the adsorption.

The Langmuir model assumes that the uptake of metal ions occurs on a homogeneous surface by monolayer sorption without interaction between sorbed ions. While the Freundlich isotherm model assumes that the adsorption occurs on a heterogeneous surface by multilayer sorption and that the adsorption amount of adsorbate increases infinitely with increasing concentration, which suggests that binding sites are not equivalent or independent.

The Langmuir model:

$$\frac{1}{q_e} = \frac{1}{q_{\max} K_L C_e} + \frac{1}{q_{\max}} \quad (6)$$

The Freundlich model:

$$q_e = K_F C_e^{1/n} \quad (7)$$

where  $q_e \text{ (mg g}^{-1}\text{)}$  and  $q_{\max} \text{ (mg g}^{-1}\text{)}$  are the amount of Cr(vi) adsorbed at equilibrium time and the maximum quantity of metal ions per unit biochar to form a complete monolayer on the surface, respectively.  $C_e \text{ (mg L}^{-1}\text{)}$  is the equilibrium solute concentration.  $K_L \text{ (L mg}^{-1}\text{)}$  is Langmuir affinity, which represents enthalpy of sorption and related to temperature.  $K_F$  and  $n$  are the Freundlich constants related to the sorption capacity and sorption intensity, respectively.

The correlation coefficient ( $R^2$ ) calculated from Langmuir and Freundlich isotherm models are listed in Table 3 and the sorption isotherms were shown in Fig. 7. It could be obviously observed that the relative parameters  $R^2$  (0.96, 0.98, 0.99) of Freundlich was higher than that (0.95, 0.95, 0.92) of Langmuir at all temperatures (298.15 K, 308.15 K, 318.15 K). These results indicated that the Cr(vi) ions sorption to the binding sites was heterogeneity sorption, which may be attributed to the active functional groups such as amino groups and carboxyl groups on the  $\beta$ -CCWB450 surface. In addition, the Freundlich model constant  $n$  at three temperature were 4.20, 4.19 and 4.29, respectively, which reflected that the adsorption between chromium ions and adsorbent was favorable ( $1 < n < 10$ ). The larger value of empirical parameter  $n$  also denotes stronger interaction between adsorbent and heavy metal. Furthermore, as seen in Table 4, the comparison of the maximum Cr(vi) adsorption capacity of various adsorbents in previous study was presented. And the prepared  $\beta$ -CCWB450 maintained much

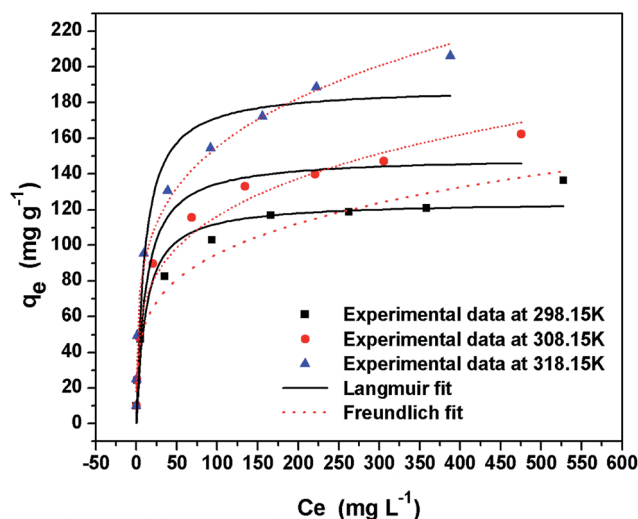
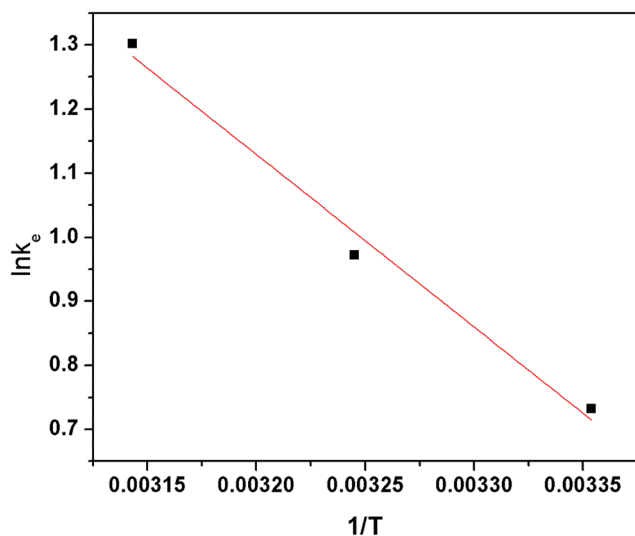


Fig. 7 Freundlich and Langmuir isotherms of Cr(vi) adsorption on  $\beta$ -CCWB450 (Cr(vi) solution volume: 50 mL; adsorbent dose: 0.1 g; contact time: 24 h; pH: 2.0).



**Table 4** Comparison of the maximum Cr(vi) adsorption capacity of various adsorbents

| Adsorbents                  | Adsorption capacity (mg g <sup>-1</sup> ) | References |
|-----------------------------|---|------------|
| Activated charcoal          | 12.87                                     | 40         |
| Activated carbon            | 36.34                                     | 41         |
| Zinc-biochar nanocomposites | 102.66                                    | 38         |
| Sugar beet tailing biochar  | 123                                       | 2          |
| β-CCWB450                   | 206                                       | This study |

**Fig. 8** Plot of  $\ln k^0$  versus  $T^{-1}$  for estimation of thermodynamic parameters for the adsorption of Cr(vi) on  $\beta$ -CCWB450 (Cr(vi) solution volume: 50 mL; adsorbent dose: 0.1 g; initial Cr(vi) concentration: 20, 50, 100, 200, 300, 400, 500, 600, 800 mg L<sup>-1</sup>; contact time: 24 h; pH: 2.0).

better Cr(vi) removal performance than many other adsorbents that reported in the literature.<sup>2,39,41,42</sup>

**3.4.3 Adsorption thermodynamic studies.** The effect of temperature on the adsorption process was investigated at three different temperatures (298.15 K, 308.15 K and 318.15 K). The thermodynamic parameters such as changes in enthalpy ( $\Delta H^0$ ), entropy ( $\Delta S^0$ ) and Gibbs free energy ( $\Delta G^0$ ) of sorption are essential in defining whether sorption is endothermic or exothermic. Three thermodynamic parameters are estimated by following relationship:

$$\Delta G^0 = -RT \ln K \quad (8)$$

$$\ln K = -\frac{\Delta H^0}{RT} + \frac{\Delta S^0}{R} \quad (9)$$

where  $K$  is the adsorption equilibrium constant.  $T$  (K) is the absolute temperature, and  $R$  (8.314 J mol<sup>-1</sup> K<sup>-1</sup>) is the gas constant.  $\Delta H^0$  (kJ mol<sup>-1</sup>) and  $\Delta S^0$  (kJ mol<sup>-1</sup> K<sup>-1</sup>) are the enthalpy change and entropy change, respectively. The values of  $\Delta H^0$  and  $\Delta S^0$  can be obtained from the slope and intercept of a plot of  $\ln K$  against  $T^{-1}$  ( $R^2 > 0.98$ ) from the Fig. 8. The results of the thermodynamic parameters were shown in Table 5.

The negative values of  $\Delta G^0$  at all different temperatures indicated that the process of the adsorption was spontaneous in nature. What's more, the apparent decrease in negative values of  $\Delta G^0$  with increasing temperature implied that the adsorption became more favorable at higher temperature. The standard enthalpy and entropy changes of adsorption were determined to be 21.91 kJ mol<sup>-1</sup> and 81.02 J K<sup>-1</sup> mol<sup>-1</sup>, respectively. The positive value of  $\Delta H^0$  proved that the adsorption was an endothermic process. The value of  $\Delta S^0$  was also positive, which suggested that the increase of randomness at the solution interface during the sorption of Cr(vi) metal ions. All the parameters may also implied that the increased temperatures provided heavy metals ions sufficient energy to overcome the diffuse layer and to be adsorbed onto biochar's interface structure.

### 3.5 The effect of ionic strength

The presence of salinity had been testified to reduce the sorption of Cr(vi) onto modified biochar.<sup>39</sup> In this study, the background ionic strength of the solutions was adjusted by NaCl. As shown in Fig. 9, the amount of Cr(vi) ions absorbed was decreased slightly with the increase of the ionic strength from 0.001 to 0.005 M. However, the removal efficiency declined to 70.5% at the higher Na<sup>+</sup> concentration of 1.0 mol L<sup>-1</sup>. The observed inverse relationship between the adsorption amount of Cr(vi) and ionic concentration suggested that salinity might have competed with Cr(vi) for sorption sites. On the other hand, the relative adsorption at higher ionic strength was not tremendously affected may also indicates that specific interactions and the formation of Cr complexation were existed besides electrostatic adsorption.

### 3.6 Desorption and regeneration analysis

Desorption is a vital process in adsorption study in order to access the economic value of the  $\beta$ -CCWB composites. Desorption study will help to regenerate the spent adsorbent so that it can be reused to adsorb Cr ions. In this experiment, desorption efficiency of the spent  $\beta$ -CCWB450 was surveyed by using 0.5 mol L<sup>-1</sup> sodium hydroxide. The adsorption-desorption cycle was repeated 5 times with same adsorbent. It was clear from Fig. 10 that the removal efficiency decreased gradually with the increasing regeneration cycles, but above 54.6% in

**Table 5** Thermodynamic parameters for Cr(vi) adsorption on  $\beta$ -CCWB450

|                                      | 298.15 K | 308.15 K | 318.15 K | $\Delta H^0$ (kJ mol <sup>-1</sup> ) | $\Delta S^0$ (kJ mol <sup>-1</sup> K <sup>-1</sup> ) | $R^2$ |
|--------------------------------------|----------|----------|----------|--------------------------------------|--|-------|
| $\ln k^0$                            | 0.732    | 0.972    | 1.301    | 21.91                                | 81.02  | 0.98  |
| $\Delta G^0$ (kJ mol <sup>-1</sup> ) | -5.155   | -6.774   | -9.716   |                                      |  |       |



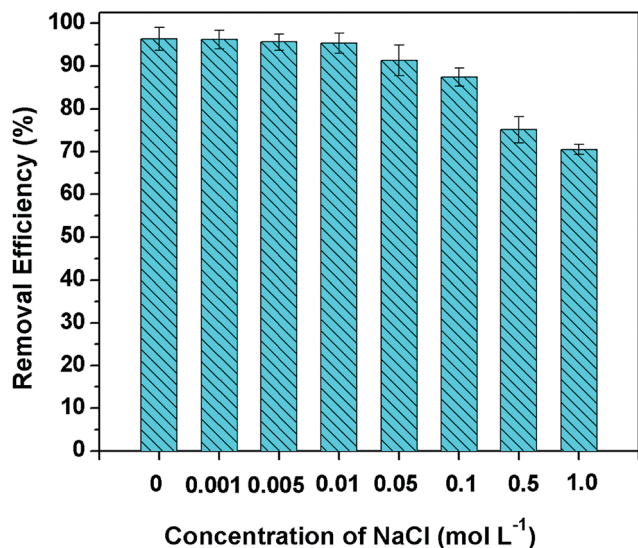


Fig. 9 Effect of different concentrations of NaCl on Cr(vi) removal by  $\beta$ -CCWB450 (Cr(vi) solution volume: 50 mL; adsorbent dose: 0.1 g; initial Cr(vi) concentration: 100 mg L<sup>-1</sup>; contact time: 24 h; pH: 2.0).

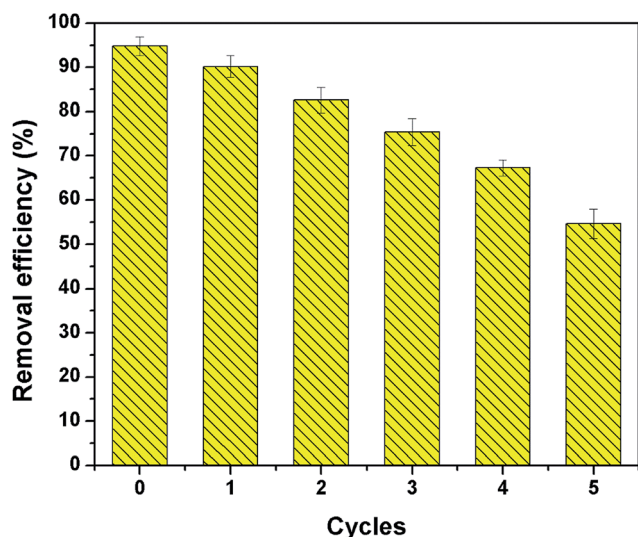


Fig. 10 Fifth consecutive adsorption–desorption cycles of  $\beta$ -CCWB450 for Cr(vi) removal (Cr(vi) solution volume: 50 mL; adsorbent dose: 0.1 g; initial Cr(vi) concentration: 100 mg L<sup>-1</sup>; contact time: 24 h; pH: 2.0).

fifth cycle, which may be a result of the decrease of specific surface area and the weakness of functional groups on  $\beta$ -CCWB. In brief, the  $\beta$ -CCWB after Cr adsorption could be regenerated with 0.5 mol L<sup>-1</sup> sodium hydroxide.

### 3.7 Reduction of Cr(vi) to Cr(III) by $\beta$ -CCWB

The concentration of Cr(vi), Cr(III) and total Cr in the solution after adsorption were measured (Fig. 11a). Cr(III), which did not exist initially, increased dramatically at the beginning of adsorption, with final Cr(III) concentration of 13.8 mg L<sup>-1</sup> and Cr(vi) concentration of 3.2 mg L<sup>-1</sup>. These results indicated that

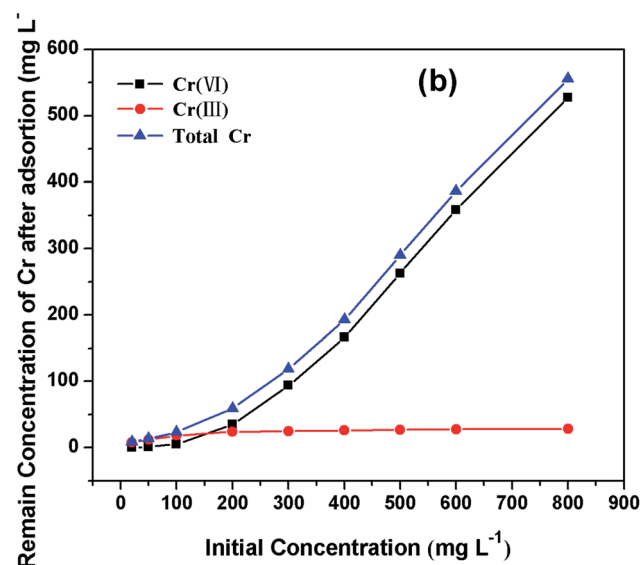
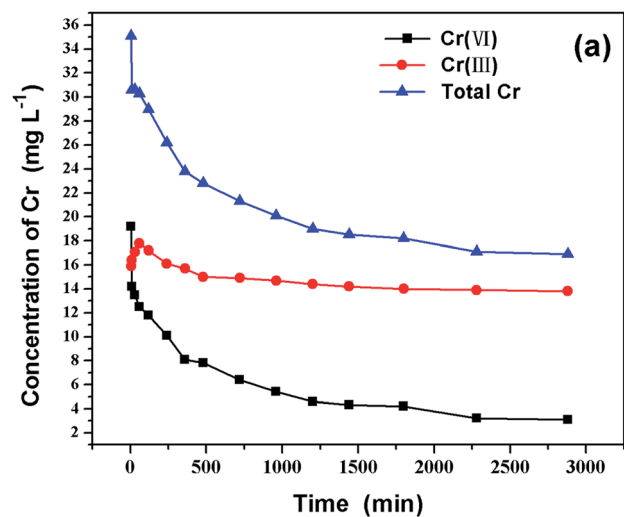


Fig. 11 (a) Time variation of Cr(III), Cr(vi) and total Cr concentration (initial Cr(vi) concentration: 100 mg L<sup>-1</sup>; Cr(vi) solution volume: 50 mL; adsorbent dose: 0.1 g; pH: 2.0), (b) initial concentration variation of Cr(III), Cr(vi) and total Cr concentration after adsorption (Cr(vi) solution volume: 50 mL; contact time: 24 h; adsorbent dose: 0.1 g; pH: 2.0).

large amount of Cr(vi) was reduced to Cr(III) when contacted with  $\beta$ -CCWB, and part of the converted Cr(III) was retained by  $\beta$ -CCWB (Fig. 3b) and the other part was released into solution.

As shown in the Fig. 11b, the removal of Cr(vi) increased with the increase of initial concentration. Interestingly, the concentration of Cr(III) after adsorption, however, remained 28.2 mg L<sup>-1</sup>, which did not raise followed the increase of initial Cr(vi) concentration. The amount of proton that disappeared in the solution was proportional to the amount of removed Cr(vi). And this results were consistent with the research of Park *et al.*<sup>43</sup> that Cr(vi) could be easily reduced to Cr(III) by positively charged functional groups. Dong *et al.*<sup>2</sup> reported that Cr(vi) was largely reduced to Cr(III) by contact with the biochar from sugar beet tailing. The reduction of Cr(vi) by organic substances is accompanied by proton consumption (eqn (10) and (11)). And this study

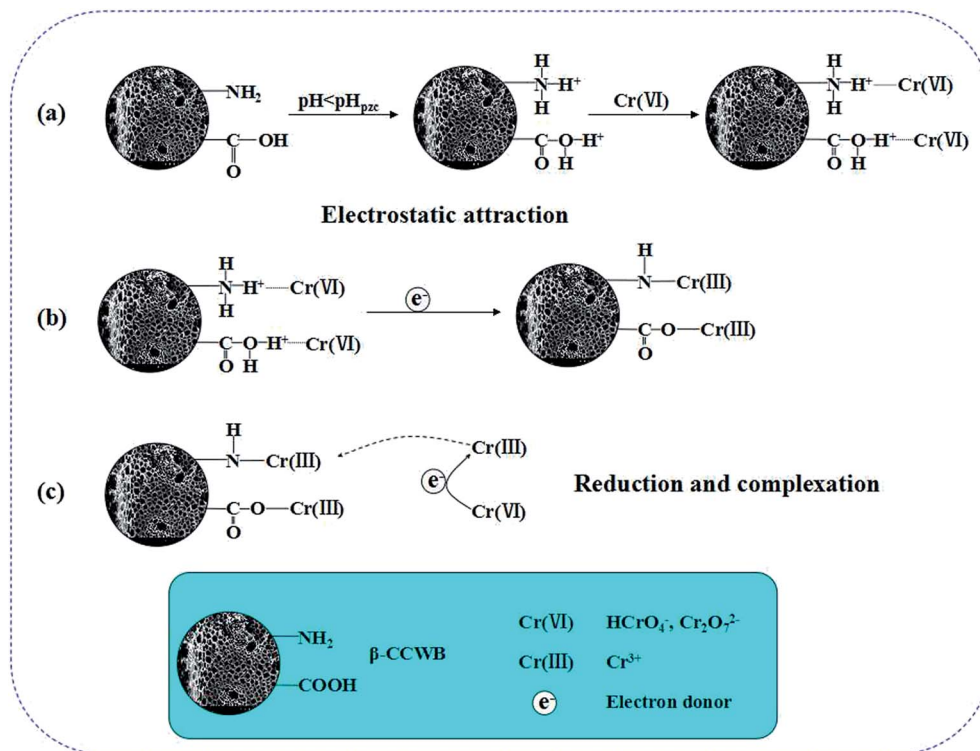
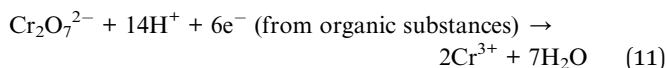
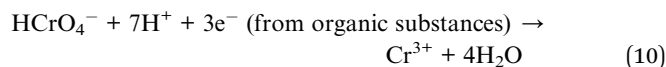


Fig. 12 Proposed removal mechanism of Cr(vi) by  $\beta\text{-CCWB}$ .

obtained the same conclusion as the reported studies, that most of the Cr bound on the  $\beta\text{-CCWB}$  was in the Cr(III) state (Fig. 3b).



### 3.8 Removal mechanism

From the FTIR spectral data, it was observed that the predominant functional groups on the  $\beta\text{-CCWB}$  were the amino groups and carboxyl groups. After metal ion adsorption, it was found that there was a significant shift in this two functional groups peak. This revealed the possible mechanism of the coordination of metal ions onto amino and carboxyl groups of  $\beta\text{-CCWB}$ . Furthermore, the XPS analysis of modified biochar (before and after adsorption) showed that chrome was successfully adsorbed to the surface of modified biochar mainly in the form of trivalent chromium. Theoretically, the  $-\text{NH}_2$  and  $-\text{COOH}$  groups on  $\beta\text{-CCWB}$  could be easily protonated and form positively charged  $-\text{NH}_3^+$  and  $-\text{COOH}^+$  groups. By the electrostatic interaction, the protonated groups on the  $\beta\text{-CCWB}$  sufficiently attracted the negatively charged  $\text{Cr}_2\text{O}_7^{2-}$  ions, resulting in the enrichment of  $\text{Cr}_2\text{O}_7^{2-}$  ions onto the surface of the  $\beta\text{-CCWB}$ .

We hypothesized that  $\beta\text{-CCWB}$  effectively removed Cr(vi) *via* electrostatic attraction of Cr(vi) coupled with Cr(vi) reduction to Cr(III) and Cr(III) complexation.<sup>2,3,43,44</sup> And it can be speculated that

three steps were involved in the adsorption process (Fig. 12). Firstly, under strongly acidic conditions, the amino and carboxyl groups on  $\beta\text{-CCWB}$  surface could be easily protonated to form  $-\text{NH}_3^+$  and  $-\text{COOH}^+$  groups, the negatively charged  $\text{Cr}_2\text{O}_7^{2-}$  and  $\text{HCrO}_4^-$  species were migrated to the positively charged surface of  $\beta\text{-CCWB}$  (protonated amino and carboxyl groups) by electrostatic interaction. Secondly, with the participation of  $\pi$  electrons donors from biochar, Cr(vi) was reduced to Cr(III) (Fig. 3b), and Cr(vi) is also reduced to Cr(III) by glutaraldehyde molecules (cross linker).<sup>44</sup> Finally, part of the converted Cr(III) was bound into  $\beta\text{-CCWB}$  surface to form stable complexed Cr(III) with functional groups, with the rest being released to the medium. Generally speaking, during the process, this new material not only acted as an adsorbent to sorb chromium but also assisted the reduction of hexavalent chromium *via* a redox reaction.

## 4. Conclusion

In this study, the walnut shell biochar modified by  $\beta\text{-CC}$  with high active surface area was successfully synthesized, the advantages of using this synthetic material as an alternative adsorbent to remove Cr(vi) from aqueous mainly based on its high removal efficiency, low cost and simple synthesis method. Characterization of  $\beta\text{-CCWB}$  indicated that the physiochemical properties (*e.g.*, surface area, porosity and thermal stability) of the biochars were significantly enhanced by the additions of  $\beta\text{-CC}$ . It is noteworthy that  $\beta\text{-CCWB}$  have an excellent adsorption and reduction capacity of Cr(vi), and the maximum adsorption capacity obtained from the optimum conditions was  $206 \text{ mg g}^{-1}$ .

The Cr(vi) removal mechanisms involved with electrostatic attraction coupled with Cr(vi) reduction and complexation. In a word, results obtained from this study demonstrated that these novel  $\beta$ -CCWB adsorbents exhibit a new opportunities for their applications in the removal of Cr(vi) ions from aqueous solution for its efficiency and both  $\beta$ -CC and biochar are low-cost and environmental friendly materials.

## Acknowledgements

This study was financially supported by the National Natural Science Foundation of China (Grant No. 41271332 and 51521006 and 51478470) and the Hunan Provincial Innovation Foundation for Postgraduate (Grant No. CX2015B090 and CX2015B095).

## References

- X. J. Tong, J. Y. Li, J. H. Yuan and R. K. Xu, *Chem. Eng. J.*, 2011, **172**, 828–834.
- X. Dong, L. Q. Ma and Y. Li, *J. Hazard. Mater.*, 2011, **190**, 909–915.
- L. Li, L. Fan, M. Sun, H. Qiu, X. Li, H. Duan and C. Luo, *Colloids Surf., B*, 2013, **107**, 76–83.
- Y. Zhou, B. Gao, A. R. Zimmerman, J. Fang, Y. Sun and X. Cao, *Chem. Eng. J.*, 2013, **231**, 512–518.
- E. Agrafioti, D. Kalderis and E. Diamadopoulos, *J. Environ. Manage.*, 2014, **133**, 309–314.
- Z. B. Zhang, X. H. Cao, P. Liang and Y. H. Liu, *J. Radioanal. Nucl. Chem.*, 2012, **295**, 1201–1208.
- D. Mohan, C. U. Pittman and P. H. Steele, *Energy Fuels*, 2006, **20**, 848–889.
- B. Chen, Z. Chen and S. Lv, *Bioresour. Technol.*, 2011, **102**, 716–723.
- R. K. Xu, S. C. Xiao, J. H. Yuan and A. Z. Zhao, *Bioresour. Technol.*, 2011, **102**, 10293–10298.
- P. Regmi, J. L. Garcia Moscoso, S. Kumar, X. Cao, J. Mao and G. Schafran, *J. Environ. Manage.*, 2012, **109**, 61–69.
- M. K. Kim, K. Shanmuga Sundaram, G. Anantha Iyengar and K. P. Lee, *Chem. Eng. J.*, 2015, **267**, 51–64.
- X. Sun and U. Ghosh, *Environ. Toxicol. Chem.*, 2008, **27**, 2287–2295.
- E. Kantarelis, W. Yang and W. Blasiak, *Fuel*, 2014, **122**, 119–125.
- X. Cao, L. Ma, B. Gao and W. Harris, *Environ. Sci. Technol.*, 2009, **43**, 3285–3291.
- J. Zhu, S. Wei, H. Gu, S. B. Rapole, Q. Wang, Z. Luo, N. Haldolaarachchige, D. P. Young and Z. Guo, *Environ. Sci. Technol.*, 2012, **46**, 977–985.
- M. Ahmad, A. U. Rajapaksha, J. E. Lim, M. Zhang, N. Bolan, D. Mohan, M. Vithanage, S. S. Lee and Y. S. Ok, *Chemosphere*, 2014, **99**, 19–33.
- M. Zhang, B. Gao, S. Varnoosfaderani, A. Hebard, Y. Yao and M. Inyang, *Bioresour. Technol.*, 2013, **130**, 457–462.
- A. Janus, A. Pelfrene, S. Heymans, C. Deboffe, F. Douay and C. Waterlot, *J. Environ. Manage.*, 2015, **162**, 275–289.
- M. Zhang, B. Gao, Y. Yao, Y. Xue and M. Inyang, *Chem. Eng. J.*, 2012, **210**, 26–32.
- M. Inyang and E. Dickenson, *Chemosphere*, 2015, **134**, 232–240.
- X. F. Tan, Y. G. Liu, G. M. Zeng, X. Wang, X. J. Hu, Y. L. Gu and Z. Z. Yang, *Chemosphere*, 2015, **125**, 70–85.
- M. Zhang, B. Gao, Y. Yao, Y. Xue and M. Inyang, *Sci. Total Environ.*, 2012, **435–436**, 567–572.
- Z. Song, F. Lian, Z. Yu, L. Zhu, B. Xing and W. Qiu, *Chem. Eng. J.*, 2014, **242**, 36–42.
- E. Agrafioti, D. Kalderis and E. Diamadopoulos, *J. Environ. Manage.*, 2014, **146**, 444–450.
- P. O. Boamah, Y. Huang, M. Hua, Q. Zhang, J. Wu, J. Onumah, L. K. Sam-Amoah and P. O. Boamah, *Ecotoxicol. Environ. Saf.*, 2015, **116**, 113–120.
- M. Vakili, M. Rafatullah, B. Salamatinia, A. Z. Abdullah, M. H. Ibrahim, K. B. Tan, Z. Gholami and P. Amouzgar, *Carbohydr. Polym.*, 2014, **113**, 115–130.
- B. Liu, X. Lv, X. Meng, G. Yu and D. Wang, *Chem. Eng. J.*, 2013, **220**, 412–419.
- W. Li, X. Liu, Q. Yang, N. Zhang, Y. Du and H. Zhu, *Food Chem.*, 2015, **184**, 99–104.
- H. Wu, J. Kong, X. Yao, C. Zhao, Y. Dong and X. Lu, *Chem. Eng. J.*, 2015, **270**, 101–109.
- L. Fan, M. Li, Z. Lv, M. Sun, C. Luo, F. Lu and H. Qiu, *Colloids Surf., B*, 2012, **95**, 42–49.
- A. Binello, G. Cravotto, G. M. Nano and P. Spaghiardi, *Flavour Fragrance J.*, 2004, **19**, 394–400.
- J. B. Dima, C. Sequeiros and N. E. Zaritzky, *Chemosphere*, 2015, **141**, 100–111.
- M. M. Zhang, Y. G. Liu, T. T. Li, W. H. Xu, B. H. Zheng, X. F. Tan, H. Wang, Y. M. Guo, F. Y. Guo and S. F. Wang, *RSC Adv.*, 2015, **5**, 46955–46964.
- W. H. Xu, S. F. Wang, Y. G. Liu, G. M. Zeng, B. H. Zheng, X. F. Tan, T. T. Li, H. Wang, F. Y. Guo and M. M. Zhang, *RSC Adv.*, 2015, **5**, 24009–24015.
- S. Stankovich, D. A. Dikin, R. D. Piner, K. A. Kohlhaas, A. Kleinhammes, Y. Jia, Y. Wu, S. T. Nguyen and R. S. Ruoff, *Carbon*, 2007, **45**, 1558–1565.
- L. Q. Xu, D. Wan, H. F. Gong, K. G. Neoh, E. T. Kang and G. D. Fu, *Langmuir*, 2010, **26**, 15376–15382.
- V. Datsyuk, M. Kalyva, K. Papagelis, J. Parthenios, D. Tasis, A. Siokou, I. Kallitsis and C. Galiotis, *Carbon*, 2008, **46**, 833–840.
- T. Y. Jiang, J. Jiang, R. K. Xu and Z. Li, *Chemosphere*, 2012, **89**, 249–256.
- C. Gan, Y. G. Liu, X. F. Tan, S. F. Wang, G. M. Zeng, B. H. Zheng, T. T. Li, Z. J. Jiang and W. Liu, *RSC Adv.*, 2015, **5**, 35107–35115.
- L. L. Wei, R. Gu and J. M. Lee, *Appl. Catal., B*, 2015, **176–177**, 325–330.
- S. Mor, K. Ravindra and N. R. Bishnoi, *Bioresour. Technol.*, 2007, **98**, 954–957.
- A. K. Giri, R. Patel and S. Mandal, *Chem. Eng. J.*, 2012, **185–186**, 71–81.
- D. Park, Y. S. Yun, J. H. Jo and J. M. Park, *Water Res.*, 2005, **39**, 533–540.
- G. N. Kousalya, M. Rajiv Gandhi and S. Meenakshi, *Int. J. Biol. Macromol.*, 2010, **47**, 308–315.